Journal of Thermal Analysis and Calorimetry (2019) 138:1207–1220
https://doi.org/10.1007/s10973-019-08794-5

Thermal analysis, structure, spectroscopy and DFT calculations of a pharmaceutical cocrystal of salicylic acid and salicylamide

Hirihattaya Phetmung[1] · Kanlayanee Musikapong[1] · Teerapol Srichana[2]

Received: 31 October 2018 / Accepted: 4 September 2019 / Published online: 19 September 2019
© Akadémiai Kiadó, Budapest, Hungary 2019

Abstract

The pharmaceutical cocrystal of salicylic acid ($C_7H_6O_3$ or H_2Sal) and salicylamide ($C_7H_7NO_2$ or SAM) was synthesized and characterized by various techniques. The differential scanning calorimetry results confirmed the eutectic fusion showing the characteristic of the endothermic sharp peak of the solidus temperature at 108 °C. X-ray crystal structure of cocrystal is orthorhombic with space group *Pna2(1)*. Cocrystal consists of H_2Sal and a distorted phenolic group of SAM. The packing diagram of cocrystal $H_2Sal{\cdot}SAM$ clearly confirmed the R_8^2 acid–amide dimer heterosynthons and other inter- and intramolecular interaction bonds to stabilize the structure. In addition, the strength of the hydrogen bonds is studied using the vibrational spectral measurements, confirming the band shifting due to the intermolecular interactions. The identity of compounds by matching the absorbance spectrum was confirmed by ultraviolet spectroscopy technique. Furthermore, the experimental studies were supported by calculation results using density functional B3LYP methods with the standard 6-311++G(d,p) basis set level. The parameters such as bond lengths, bond angles and Mulliken atomic charges values have been calculated and compared, confirmed the interactions and charge transfers. The frontier molecular orbitals (HOMO–LUMO) illustrated the lower band-gap value suggesting the possible pharmaceutical activity of this as obtained $H_2Sal{\cdot}SAM$ cocrystal.

Keywords Pharmaceutical cocrystal · Salicylic acid · Salicylamide · Computational chemistry · Density functional theory · Acid–amide dimer heterosynthons

Introduction

Pharmaceutical cocrystallization is often considered for the development of API drugs [1–11]. This method is about searching the suitable solid form which can enhance the specific physical properties such as solubility, bioavailability, stability, etc. without affecting the biological activity of the drug [1–9]. In general, cocrystals are formed through noncovalent interaction bonds (primarily hydrogen bonding), π–π stacking, van der Waals interactions and other weak interactions [1–11].

Salicylic acid or 2-hydroxybenzoic acid ($C_7H_6O_3$ or H_2Sal) is nonsteroid anti-inflammatory drug (NSAID) that shows analgesic effects [12–15]. Salicylamide 2-hydroxybenzoic acid ($C_7H_7NO_2$ or SAM) is not only the salicylic derivative but also the NSAID. It is the weak antifungal, antibacterial actions and keratolytic [2, 9, 15]. Salicylic acid and salicylamide are phenolic compounds in which both contain the phenolic hydroxyl group (Ph-OH) [2]. Moreover, carboxyl (C(O)–OH) group of salicylic acid and carboxamide (C(O)–NH_2) group of salicylamide are the key tools to generate cocrystal via the concept of supermolecular sythons such as carboxylic–carboxylic, amide–salicylamide and carboxylic–salicylamide denoted as types (**I**), (**II**) and (**III**), respectively (see Fig. 1) [3–11].

✉ Hirihattaya Phetmung
tayaphetmung@yahoo.com

Kanlayanee Musikapong
Riam_321@hotmail.com

Teerapol Srichana
teerapol.s@psu.ac.th

[1] Inorganic and Materials Chemistry Research Unit, Faculty of Science, Thaksin University, Muang, Songkhla 90000, Thailand

[2] Department of Pharmaceutical Technology, Faculty of Pharmaceutical Sciences, Prince of Songkla University, Hat Yai, Songkhla 90112, Thailand

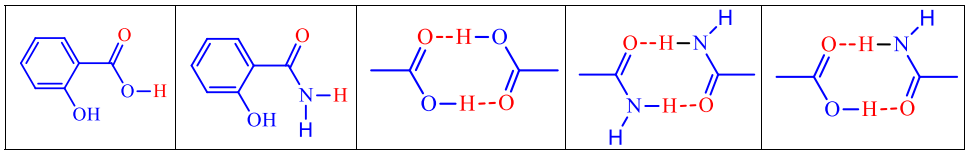

Fig. 1 The chemical structures of H_2Sal and SAM and some probable molecular synthons

The cocrystal of salicylic acid and salicylamide has been reported with other molecules for the purpose of increasing pharmaceutical physicochemical properties [3, 9, 10, 15, 16]. The example cocrystals of salicylic acid are with ethenzamide [3] and benzamide [9]. The cocrystals of salicylamide are with itself as homosynthon [10, 15], 3,5-dinitrobenzoic acid [4] and piperidine-3-carboxylic acid [16].

In addition, the pharmaceutical individual crystals and cocrystals of salicylic acid and salicylamide have been studied in detail not only experimentally but also from a theoretical point of view [3, 4, 10, 15–21]. Computational chemistry is especially used as a tool to understand the physiochemical properties, such as the weak interaction, molecular synthons or motifs as shown in Fig. 1 [10, 21, 22].

However, to the best of our knowledge, there is no report on both preparation and computational chemistry calculations of such cocrystal of salicylic acid and salicylamide ($H_2Sal{\cdot}SAM$). Therefore, the main objective of this work is to combine the experimental and theoretical investigations for understanding the preparation, molecular interactions and other relative properties and aiming for a drug design.

Experimental

Preparation of compounds

All the chemicals were obtained commercially and used without further purification. For better understanding and accurate data, we recrystallized the starting materials H_2Sal and SAM.

H_2Sal was obtained by 5 mL of methanol solvent-drop grinding of salicylic acid (0.14 g, 0.01 mol). When the solution was allowed to evaporate to dryness, crystals were obtained within a day with 85% yield.

SAM was also obtained by 5 mL of methanol solvent-drop grinding of salicylamide (0.27 g, 0.02 mol). When the solution was allowed to evaporate to dryness, crystals emerged after 2 days with 80% yield.

Cocrystal $H_2Sal{\cdot}SAM$: Actually, several attempts were also done to obtain cocrystals. We have tried multiple methods to purify or prepare pharmaceutical compounds such as slow solvent evaporation, cooling, solvent-drop grinding [23] and also slurring techniques [24]. Fortunately, the methods reported in this work gave the single crystals which were suitable for X-ray diffraction studies.

In the typical procedure, pharmaceutical cocrystal $H_2Sal{\cdot}SAM$ was synthesized in the 1:2 mole ratio by the solvent evaporation method. Salicylic acid (0.14 g, 0.01 mol) and salicylamide acid (0.27 g, 0.02 mol) were dissolved in 20 mL of ethanol and continuously stirred for 1 h at room temperature. Then, the solution was filtered off and allowed to slowly evaporate at ambient temperature; single cocrystals were obtained within a week with 83% yield.

Physical measurements

The elemental analyses for C, H, and N were performed on a Perkin-Elmer 240 analyzer. The FT-IR spectra were recorded as KBr pellets on a Perkin-Elmer FT-IR spectrometer in the 4000–400 cm^{-1} region.

Differential scanning calorimetry (DSC) analysis was carried out using a DSC 204 F1 Phoenix differential scanning heat flux calorimeter (NETZSCH, Germany) with a high sensitivity m-sensor. Sample mass was usually in the range of 5–9 mg. The heating rate is about 10 °C min^{-1} in argon gas and cooled with liquid nitrogen gas. The UV–Visible spectra are recorded using a Shimadzu UV-1700 spectrophotometer which covered the range of 500–200 nm.

Single-crystal X-ray structure determination

X-ray diffraction studies were carried out using a Bruker APEX2 CCD diffractometer equipped with graphite-monochromated Mo Kα radiation (λ = 0.71073 Å). The SAINT program of the SHELXTL software package was used for data collection, cell refinement and data reduction [25]. The SADABS program applied only cocrystal refinement. The structures were solved by direct methods using Shelxs97, and the structure refined against F^2 for all reflections by full-matrix methods. The phenolic oxygen atom was examined for the dynamic disorder and then restrain. However, all non-hydrogen atoms were refined anisotropically and the hydrogen atoms were placed in geometric positions and refined as the riding model atoms with C–H = 0.93 Å and $U_{iso}(H) = 1.2\ U_{eq}(C)$. Program Mercury and Diamond were used to demonstrate the figures [26].

Computational details

For the accuracy, precision and reliability, the initial structure geometries were started from experimental (single-crystal X-ray structure) data. In order to obtain the stable conformer, the self-consistent field (SCF) energy calculation is performed with the HF and DFT methods. From SCF energy calculation, we assumed that the most stable conformer structure is the same as the obtained molecules from X-ray structure determination. We found that DFT calculations with the hybrid density functional method 6-311++G(d,p) are the suitable method (see Table 2), for the prediction and evaluation of organic molecules, which matched well with many literature reviews [9, 10, 15–22].

This hybrid density functional method from the Gaussian 98 program is expected to provide sufficient quantitative accuracy for present purposes [27]. The optimized structure parameters were also used in the computed vibration frequency at the same level to characterize all stationary points as minima. The natural bond orbital (NBO) calculation was also carried out at the same level to get more detailed information about the chemical bonds of the molecule. The frontier molecular orbitals (FMO) has been computed and analyzed. The molecular orbitals were generated using the GaussView program in Gaussian 98 software package [27].

Results and discussion

Experimental pharmaceutical cocrystal $H_2Sal{\cdot}SAM$

H_2Sal, SAM and cocrystal $H_2Sal{\cdot}SAM$ were obtained. For the cocrystal $H_2Sal{\cdot}SAM$, we successfully prepared the crystals from the 1:2 (salicylic acid: salicylamide) mole ratio with solution crystallization after we have been tried several reactions by changing the preparation methods such as solid–solid grinding [6, 7, 23], solvent-drop grinding with varying the mole ratios [2, 3, 6, 7]. This is to confirm that the solvent evaporation method can be broken and reformed under this condition.

The crystals of H_2Sal, SAM and $H_2Sal{\cdot}SAM$ exhibit the colorless needle-like, colorless plate-like and long plate-like morphologies, respectively, as shown in Fig. 2.

Experimental DSC results

DSC is used as the tool to understand the cocrystalline phase characterization and identification. The DSC thermogram of cocrystal and its starting materials H_2Sal and SAM are illustrated in Fig. 3. The DSC curve of cocrystal exhibits the endothermic peaks, similar to those in cocrystal of salicylamide with acetamidobenzoic acid and other similar cocrystals [3, 5–11].

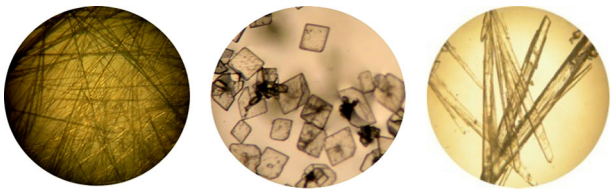

Fig. 2 The crystal morphology of H_2Sal (left), SAM (middle) and $H_2Sal{\cdot}SAM$ (right)

The intense and sharp endothermic peak confirm the cocrystal changing from solid to liquid state at 108 °C (enthalpy = 162.00 J g^{-1}), as the melting point of the solid. The cocrystal melting which is lower temperature than those of their starting materials (155 °C of H_2Sal and 137 °C of SAM), confirming the eutectic fusion [6, 7, 9, 28, 29]. Moreover, the crystallinity of this process is about 100%, supporting the solubility [9, 30].

Experimental Single-crystal structure of pharmaceutical cocrystal H_2Sal, SAM and $H_2Sal{\cdot}SAM$

The molecular structures of H_2Sal, SAM and $H_2Sal{\cdot}SAM$ are shown in Fig. 4. The crystal structure parameters are listed in Table 1.

H_2Sal has been previously reported in both experimental and theoretical studies [13, 18]. In this work, H_2Sal crystallizes in monoclinic crystal system with a space group $P2_1/c$ and appears as ortho hydroxyl benzoic acid which is in a different form from the previous reports but in the

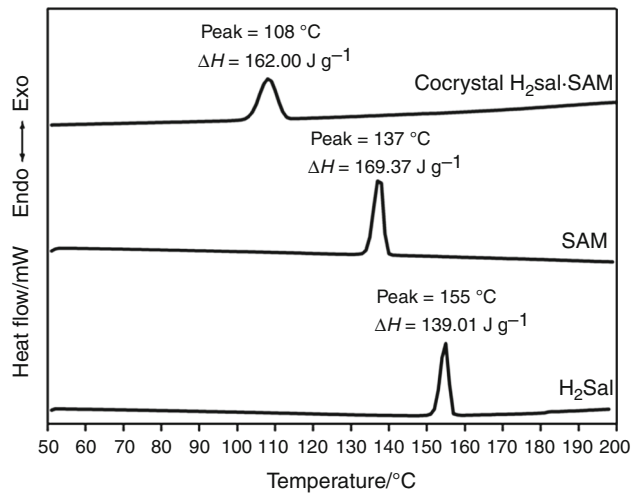

Fig. 3 The DSC curve of cocrystal $H_2Sal{\cdot}SAM$

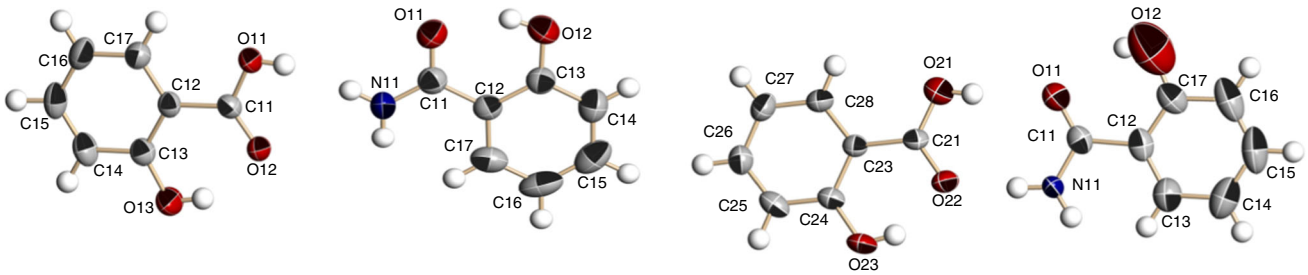

Fig. 4 The structure of H_2Sal (left), SAM (middle) and cocrystal $H_2Sal{\cdot}SAM$ (right) plot at approximately 30% with atom-numbering scheme

same form with some experimental reports and the most stable optimization structures.

SAM is also crystallized in the same crystal system and a space group as H_2Sal [14]. The replacement of amide (NH_2) group to O–H of COOH group yields the SAM structure.

$H_2Sal{\cdot}SAM$ is a cocrystal which crystallizes in orthorhombic crystal system with a space group $Pna2_1$. As seen, the phenolic hydroxyl (Ph-OH) is disordered which may effect in hydrogen bond interactions and the rest of the molecules. This phenomenon clearly confirmed by DSC results.

Moreover, the apparent of Flack's absolute structure parameter (0.8(18)) confirms that cocrystal has chirality which is good for the pharmaceutical selectivity and activity [9].

Experimental and DFT calculation results of structure parameters

Bond, angles and torsion angles of these three crystals structures

Selected bond lengths, bond angles and torsion angles from experimental and theoretical studies are listed in Table 2. The hydrogen bond and weak interactions are shown in Table 3 and Figs. 5–7.

Indeed, H_2Sal consists of three organic functional groups: a carboxylic (COOH), phenolic hydroxyl (Ph-OH) groups and an aromatic cycle. In this work, the carboxylic C=O bond distances are about 0.05(2) Å shorter than the phenolic hydroxyl distances (1.3066(16) Å vs. 1.3066(16) Å). In contrast, the hydroxyl group has longer bond distances (0.96(2)Å vs. 0.93(2) Å).

For SAM, the phenolic hydroxyl (Ph-OH), the carboxylic C=O bond distances are about the same as those in H_2Sal.

As seen in Table 2, the structure parameters such as bond lengths, bond angles and torsion angles of cocrystal are shorter or lower than its starting materials, confirming the cocrystal stability than free molecules, for example, the 1.3066(16) Å vs. 1.302(4) Å carboxylic C=O bonds [9].

The hydrogen synthons and weak interactions

As seen in Table 3, the experimental weak interactions of these three compounds are summarized, except the last column of calculated d(H···A), and the experimental structure is illustrated in Figs. 5–7. Undoubtedly, hydrogen bonding plays the important roles to form the building block units known as supramolecular synthons. The calculated weak interactions in all structures are systematic higher than experimental results, because of the gas-phase calculations.

The packing diagram revealed that H_2Sal has not only intramolecular hydrogen bonding (O13–H13···O12 of 1.779 Å) but also intermolecular hydrogen bonding (O11–H11···O12 of 1.698 Å) which is similar to the previous reports [3, 6–10]. The intermolecular interaction was R_8^2 acid–acid dimer homosynthon which is a typical form for salicylic acid [3], as shown in Fig. 5.

Surprisingly, the packing diagram of SAM also revealed the R_8^2 amide–amide dimer homosynthon and the R_{12}^4 amide–amide tetramer homosynthon which has not stated in the previous report [3, 10, 11]. The R_{12}^4 tetramer synthon formed through N11–H11···O12 of 2.455 Å intermolecular hydrogen bonds. Overall intra- and intermolecular interaction hydrogen bonding is longer than those of H_2Sal as listed in Table 3 and Fig. 6.

The supramolecular heterosynthon occurred in cocrystal $H_2Sal{\cdot}SAM$ which is the R_8^2 acid–amide dimer heterosynthons. In this case, the dimer motif is augmented by the amide–acid dimer established through N11–H11···O22 of 1.820 Å and O21–H21···O11 of 2.105 Å and O21–H21···O11 of 2.105 Å. The phenolic O–H···O intramolecular hydrogen bonding of H_2Sal is 0.24 Å shorter than that of SAM, as shown in Fig. 7 and Table 3.

Experimental and DFT calculation results of FT-IR spectra

In order to understand weak interactions, FT-IR spectroscopy is the perfect tool. For the extension of our work, H_2Sal, SAM and $H_2Sal{\cdot}SAM$ have been performed by DFT

Table 1 Crystal data and structure refinement for H_2Sal, SAM and cocrystal $H_2Sal{\cdot}SAM$

Identification code	H_2Sal	SAM	$H_2Sal{\cdot}SAM$
CCCD code	1545141	1545142	1545143
Empirical formula	$C_7H_6O_3$	$C_7H_7NO_2$	$C_{14}H_{13}NO_5$
Formula weight	138.12	137.14	275.25
Wavelength/°	0.71073	0.71073	0.71073
Crystal system	Monoclinic	Monoclinic	Orthorhombic
Space group	*P2(1)/c*	*P2(1)/c*	*Pna2(1)*
a/°	4.9067(8)	6.543(2)	21.5053(11)
b/°	11.218(2)	15.569(6)	5.0264(3)
c/°	11.537(2)	7.104(3)	12.1428(5)
α/°	90	90	90
β/°	90.806(10)	113.646(9)	90
γ/°	90	90	90
V/Å^3	635.0(2)	662.9(4)	1312.57(12)
Z	4	4	4
Density (calculated)/mg/m^3	1.445	1.374	1.393
Absorption coefficient/mm^{-1}	0.114	0.102	0.107
F(000)	288	288	576
Crystal size/mm^3	0.56 × 0.16 × 0.12	0.28 × 0.18 × 0.12	0.32 × 0.24 × 0.16
θ range/°	3.53–26.09	3.39–25.72	2.53–25.10
Index ranges	$-6 \le h \le 5$	$-7 \le h \le 7$	$-25 \le h \le 25$,
	$-12 \le k \le 13$	$-18 \le k \le 18$	$-4 \le k \le 6$,
	$-14 \le l \le 13$	$-8 \le l \le 8$	$-14 \le l \le 14$
Reflections collected	3145	7943	8446
Independent reflections	1246 [R(int) = 0.0176]	1253 [R(int) = 0.0423]	2314 [R(int) = 0.0233]
Completeness to θ = 26.09°	98.9%	99.8%	99.9%
Absorption correction	None	None	None
Refinement method	Full-matrix least squares on F^2	Full-matrix least squares on F^2	Full-matrix least squares on F^2
Data/restraints/parameters	1246/0/116	1253/0/91	2314/1/182
Goodness-of-fit on F^2	1.031	1.101	1.079
Final R indices [$I > 2\sigma$ (I)]	R_1 = 0.0336	R_1 = 0.0479	R_1 = 0.059
	ωR_2 = 0.0866	ωR_2 = 0.1199	wR_2 = 0.1596
R indices (all data)	R_1 = 0.0476	R_1 = 0.0782	R_1 = 0.0675
	ωR_2 = 0.0955	ωR_2 = 0.1365	wR_2 = 0.1692
Absolute structure parameter			0.8(18)
Extinction coefficient	0.014(5)		0.013(4)
Largest diff. peak and hole/e Å^{-3}	0.141 and − 0.135	0.230 and − 0.303	0.306 and − 0.338

with 6-311++G(p,d). As the results shown in Figs. 8 and 9, the theoretically computed values are typically higher than those of experimental data because of gas-phase calculation which is in very good agreement with experimental results and the previous studies of salicylic acid have been reported [17–20].

Actually, the crystal structure of H_2Sal contains only three major functional groups which are carboxylic groups, aromatic hydrogen and phenolic functional groups, whereas SAM consists of the primary amide group instead of hydroxyl group [8, 17]. $H_2Sal{\cdot}SAM$ has the combination of H_2Sal and SAM functional groups.

Carboxylic group

Carboxylic group (–COOH) consists of carbonyl (C=O) and hydroxyl (O–H) groups. For the O–H vibration, it is the key role and extremely important to form the hydrogen bonding, indicating the broad band between 3600 and 3300 cm^{-1}.

Table 2 Comparison of selected bond lengths/Å, bond angles/° and torsion angles/° from experimental and theoretical studies

H_2Sal				SAM				$H_2Sal{\cdot}SAM$			
Parameter	Exp.	HF	DFT	Parameter	Exp.	HF	DFT	Parameter	Exp.	HF	DFT
O(11)–C(11)	1.3066(16)	1.3221	1.3489					O(21)–C(21)	1.302(4)	1.300	1.351
O(11)–H(11)	0.96(2)	0.946	0.9687					O(21)–H(11)	0.82	0.960	0.965
O(12)–C(11)	1.2365(2)	1.1972(1)	1.226					O(22)–C(21)	1.269(4)	1.200	1.239
O(12)–H(13)		1.8599	1.7617					O(22)–H(11A)	1.820	2.040	1.767
O(13)–C(13)	1.3533(2)	1.3779	1.3429					O(23)–C(24)	1.345(4)	1.320	1.348
O(13)–H(13)	0.93(2)	0.9492	0.9812					O(23)–H(13)		0.940	0.980
C(11)–C(12)	1.4590(12)	1.4721	1.4641								
				O(11)–C(11)	1.247(2)	1.2102	1.2406	O(11)–C(11)	1.202(4)	1.320	
				O(12)–H(12)	0.802(2)	0.980	0.989	O(12)–H(12)	0.8200	0.950	0.999
				N(11)–C(11)	1.302(3)	1.3479	1.359	N(11)–C(11)	1.319(4)	1.330	1.323
				N(11)–H(3)	0.860(2)	0.9932	1.0075	N(11)–H(11A)	0.8600	0.980	0.999
				N(11)–H(4)	0.860(2)	0.9879	1.0038	N(11)–H(11B)	0.8600	0.990	0.999
				O(12)–C(13)	1.354(2)	1.3256	1.3398	C(17)–O(12)	1.307(8)	1.452	1.421
C(11)–O(11)–H(11)	109.7(11)	108.41	106.88					C(21)–O(21)–H(21)	109.5	111.21	
C(13)–O(13)–H(13)	105.7(14)	110.56	108.06					C(24)–O(23)–H(23)	109.5	109.92	110.04
O(12)–C(11)–O(11)	121.70(12)	121.03	120.73					O(22)–C(21)–O(21)	120.3(3)	124.5	121.52
O(12)–C(11)–C(12)	122.53(12)	124.48	124.48					O(22)–C(21)–C(23)	119.1(3)	122.99	123.22
O(11)–C(11)–C(12)	115.77(12)	114.48	114.7793(2)					O(21)–C(21)–C(23)	120.7(3)	114.97	120.91
				C(13)–O(12)–H(17)	109.50	109.63	106.88	C(17)–O(12)–H(12)	109.5	109.75	110.64
				C(11)–N(11)–H(3)	119.43	116.99	117.30	C(11)–N(11)–H(3)	120.00	116.99	117.30
				C(11)–N(11)–H(4)		124.14	123.70	C(11)–N(11)–H(4)	120.00	124.14	123.70
				H(3)–N(11)–H(4)		118.86	118.99	H(3)–N(11)–H(4)	120.00	118.86	118.99

Table 3 Experimental and some calculated weak interactions of H_2Sal, SAM and $H_2Sal{\cdot}SAM$

D–H	d(D–H)	d(H···A)	<DHA	d(D···A)	A	Cal. d(H···A)
H_2Sal						
O13–H13	0.932	1.779	148.02	2.617	O12	1.870
O11–H11	0.959	1.698	177.02	2.656	O12 [− x, − y + 1, − z + 1]	1.882
SAM						
O12–H12	0.820	1.822	146.61	2.547	O11	1.923
N11–H11A	0.860	1.946	170.46	2.797	O11 [− x + 2, − y + 1, − z + 3]	2.056
N11–H11B	0.860	2.445	142.56	3.172	O12 [x − 1, y, z]	2.556
$H_2Sal{\cdot}SAM$						
N11–H11A	0.860	1.820	170.10	2.671	O22	1.980
N11–H11B	0.860					
O21–H21	0.820	2.105	172.98	2.920	O11	2.255
O23–H23	0.820	1.787	148.01	2.520	O22	1.892
O12–H12	0.820	2.027	129.40	2.625	O11	2.168

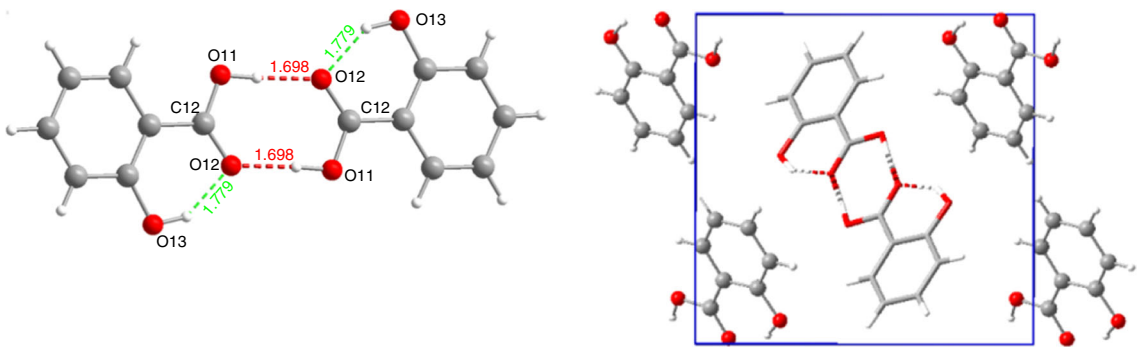

Fig. 5 The R_8^2 acid–acid dimer homosynthon of salicylic acid showing the numbering of the asymmetric unit in the crystal

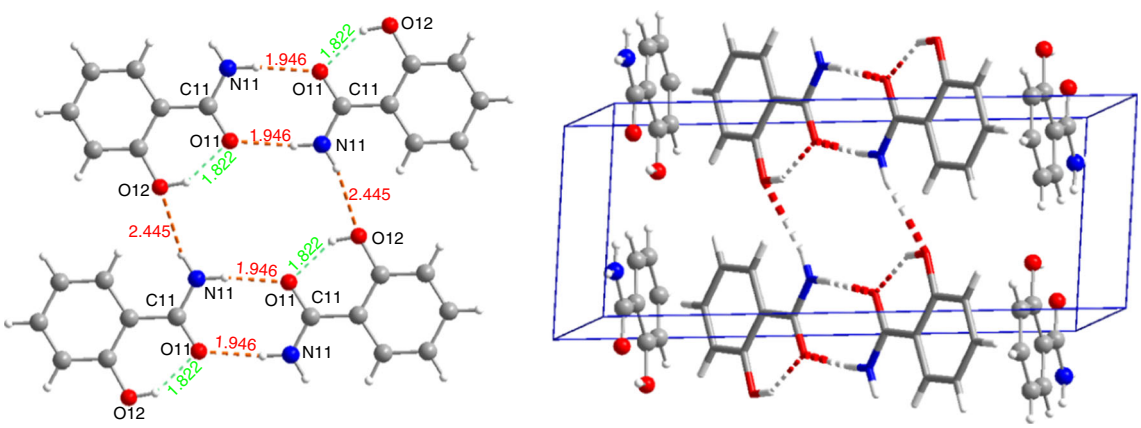

Fig. 6 The R_8^2 amide–amide dimer and R_{12}^4 amide–amide tetramer homosynthons of salicylamide showing the numbering of the asymmetric unit in the crystal

In this work, all the experimental spectra have the very broad peak of carboxylic acid covering the region of 2500–3500 cm^{-1} indicating the dimer hydrogen bonds [3, 8, 9, 15, 17], supporting the single-crystal X-ray structures data. The overriding spectra are normally centered at around 3000 cm^{-1}. This is to confirm that H_2Sal, SAM can form not only monomer but also dimer molecules as the R_8^2 acid–acid dimer of H_2Sal covering the region of

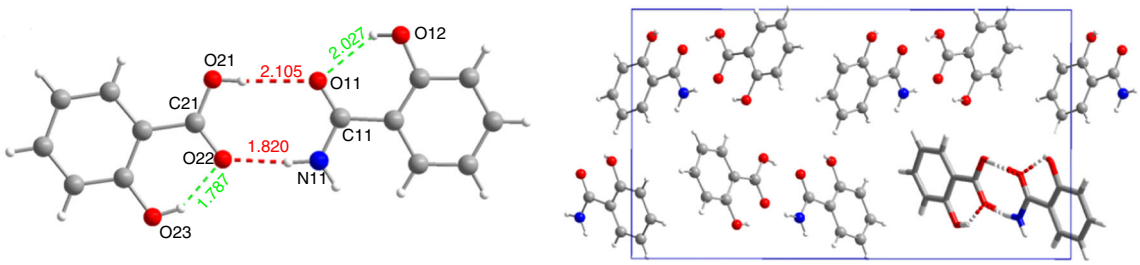

Fig. 7 The R_8^2 acid–amide dimer heterosynthon of cocrystal showing the numbering of the asymmetric unit in the crystal

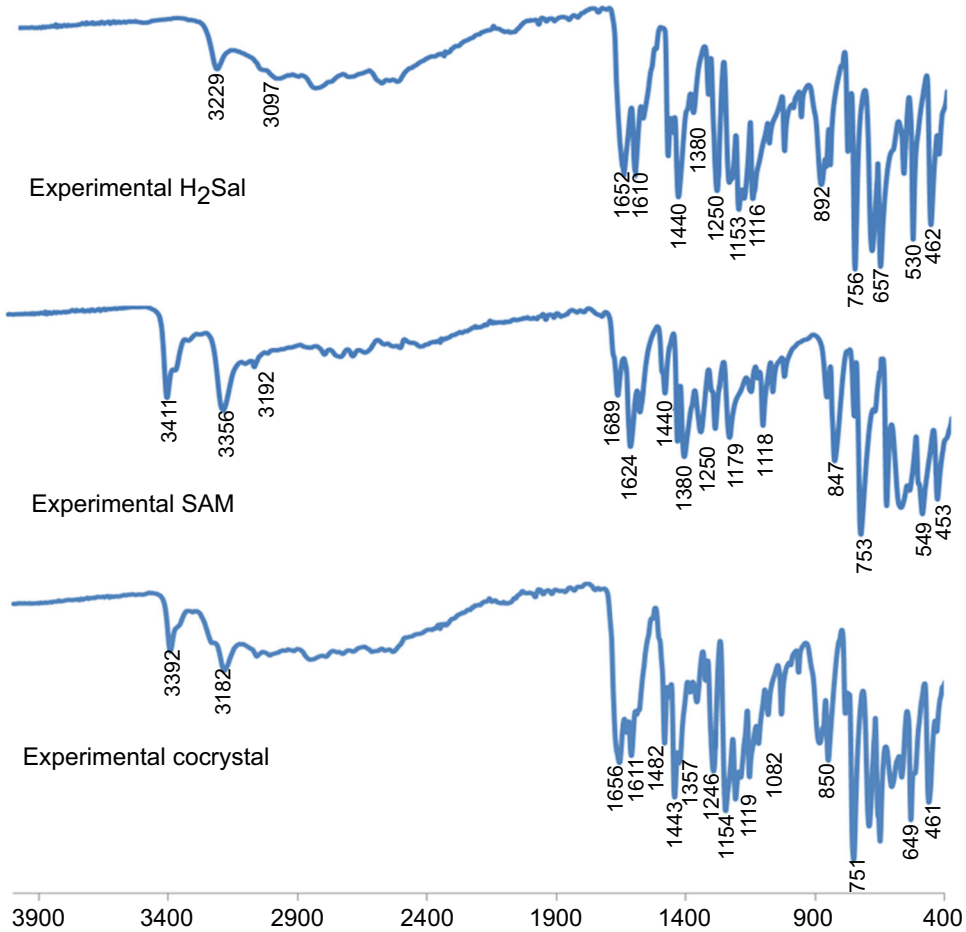

Fig. 8 FT-IR spectra of experimental H_2Sal, SAM and cocrystal ($H_2Sal{\cdot}SAM$)

2500–3500 cm^{-1} indicating the dimer hydrogen bonds [3, 9, 15, 17], supporting the single-crystal X-ray structures data. The overriding spectral is normally centered at around 3000 cm^{-1}. This is to confirm that H_2Sal, SAM can form not only monomer but also dimer molecules as the R_8^2 amide–amide dimer homosynthons SAM [3, 17, 19, 21].

Surprisingly, the experimental spectra of cocrystal $H_2Sal{\cdot}SAM$ appear at the weak broad band in the region of 2300–2800 which is lower than those of free H_2Sal and SAM, strongly confirm the R_8^2 acid–amide dimer heterosynthons of cocrystal $H_2Sal{\cdot}SAM$. In sum, during the cocrystallization, the band was shifted to the lower band.

The O–H in-plane bending and out of the plane bending vibrations of H_2Sal, SAM and $H_2Sal{\cdot}SAM$ appear in the general region of 1380–1440 cm^{-1} and 549–1179 cm^{-1}. Surprising, the O–H in-plane bending of the dimer wavenumbers are increasing, may be affected by the carboxyl group.

For the carbonyl (C=O) group, the stretching vibration of H_2Sal, SAM and $H_2Sal{\cdot}SAM$ are 1652 cm^{-1}, 1689 cm^{-1} and 1678 cm^{-1} which are in the region 1650–1715 cm^{-1} [15]. As the normal expectation, the wavenumber of cocrystals is lower than those of free H_2Sal

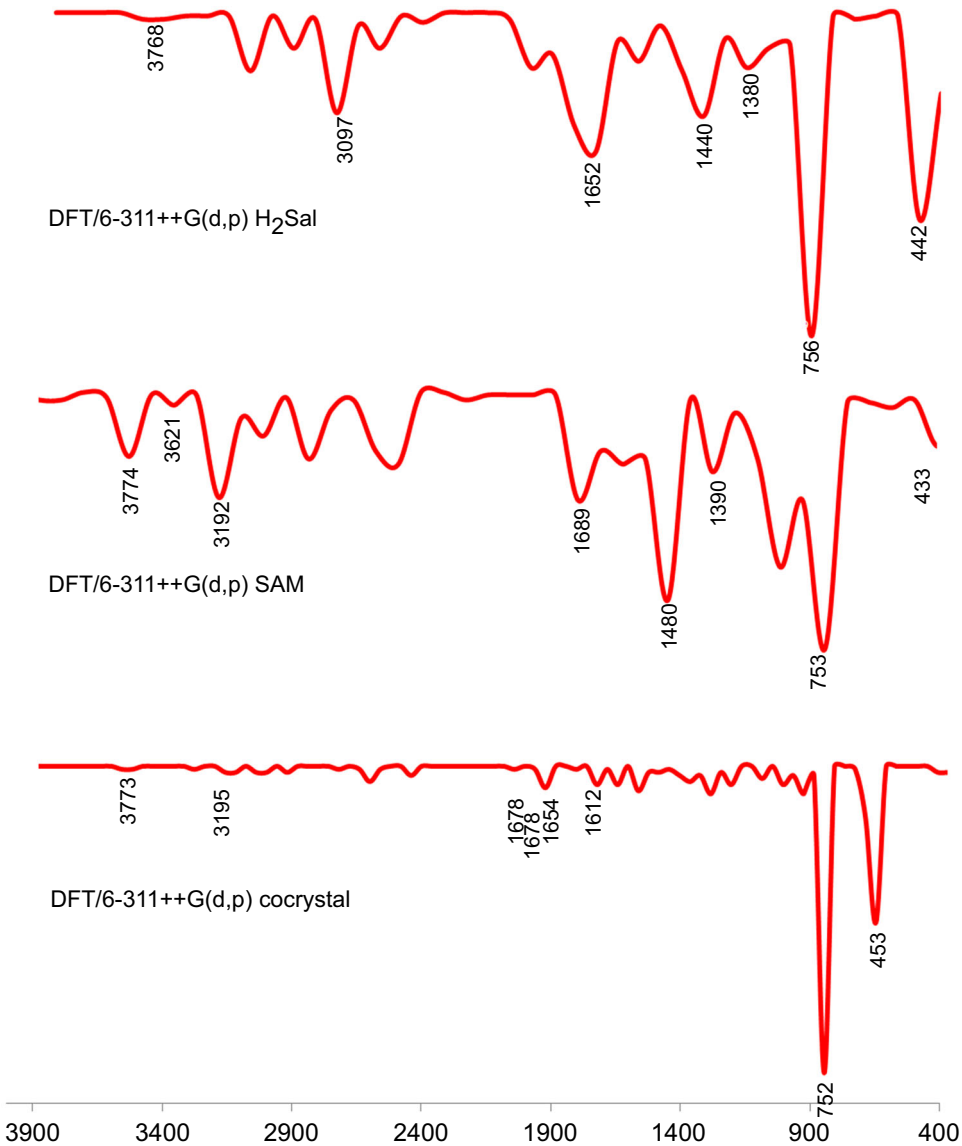

Fig. 9 FT-IR spectra of DFT calculation of H_2Sal, SAM and cocrystal ($H_2Sal{\cdot}SAM$)

and SAM, due to the intermolecular interactions, appearing at the bridging mode of hydrogen bond [15–20].

Phenolic functional groups

The experimental phenolic O–H in-plane bending vibrations of H_2Sal and SAM are in the typical wavenumbers of 1100 cm^{-1}–1250 cm^{-1} [15–21]. In the cocrystal, the signal appears at 1119 cm^{-1}. There are the peaks at lower than 500 cm^{-1} (462 cm^{-1} of H_2Sal, 453 cm^{-1} of SAM) which are identified and assigned to the combination of CO···H and ν(O···H), the corresponding theoretical peaks are at 442 cm^{-1} of H_2Sal, 433 and 415 cm^{-1} of SAM and 453 cm^{-1} of cocrystals [17, 21, 22].

Aromatic hydrogen group

The observed spectra peaks appearing at 3097 cm^{-1}, 3192 cm^{-1} and 3192 cm^{-1} are corresponding to aromatic C–H stretching vibration of H_2Sal, SAM and $H_2Sal{\cdot}SAM$, respectively [9, 19]. The peaks during 675 cm^{-1}–900 cm^{-1} belong to C–H 'oop' which are 756 cm^{-1} (H_2Sal), 753 cm^{-1} (SAM) and 752 cm^{-1} ($H_2Sal{\cdot}SAM$) [9].

Primary amide group

The observed primary amide of SAM and $H_2Sal{\cdot}SAM$ has two peaks which are asymmetric (3773 cm^{-1} vs. 3411 cm^{-1}) and symmetric vibrations (3621 cm^{-1} vs. 3356 cm^{-1}) [9, 15, 19, 21]. The significant decrease in asymmetric amide in cocrystal extremely confirmed this

Table 4 The UV spectra of H_2Sal, SAM and $H_2Sal{\cdot}SAM$

Compounds	Peak I/nm./intensity	Peak I/nm./intensity	References
H_2Sal	231 (1.78)/123.77 kcal mol^{-1}	303 (0.774)/94.36 kcal mol^{-1}	[29]
	233 (1.78/122.71 kcal mol^{-1}	306 (0.840)/93.44 kcal mol^{-1}	This work
SAM	235/121.67 kcal mol^{-1}	305/93.74 kcal mol^{-1}	[32]
$H_2Sal{\cdot}SAM$	223(1.78)/128.21 kcal mol^{-1}	306 (0.729)/93.44 kcal mol^{-1}	This work
Transition	$n \rightarrow \sigma^*$	$\pi \rightarrow *$	

amide group is involving with the N–H···O bonding [9], creating R_8^2 acid–amide heterodimer of ($H_2Sal{\cdot}SAM$). The N–H bending peaks are typical in the region of 1650–1560 cm^{-1}, with 1624 cm^{-1} and 1610 cm^{-1} (SAM) and 1654 cm^{-1} and 1612 cm^{-1} ($H_2Sal{\cdot}SAM$).

Experimental and DFT calculation results of ultraviolet (UV) spectra

UV spectroscopy was performed in order to identify the functional group or confirm the identity of compounds by matching the absorbance spectrum. All UV spectra of H_2Sal, SAM and $H_2Sal{\cdot}SAM$ show the intense at lower wavelengths and weak peaks at higher wavelengths which are 233 and 303 (H_2Sal), 231 and 303 nm (SAM) and 223 and 306 nm ($H_2Sal{\cdot}SAM$). These peaks are corresponded with $n \rightarrow \sigma^*$ and $\pi \rightarrow \pi*$ [4, 31]. The comparison of experimental results is shown in Table 4. Surprisingly, these experimental phenomena indicate about the same wavelengths, supporting an unchanged structure. The calculated experimental energies of $n \rightarrow \sigma^*$ and $\pi \rightarrow \pi*$ are illustrated in the range of 121.67–128.21 kcal mol^{-1} and 93.44–94.36 kcal mol^{-1}, respectively.

DFT calculation results of HOMO–LUMO energy

Molecular energy from the optimization energy at B3LYP/6-311++G(d,p) level may give us the idea of some properties, such as stability. By comparing the energy of H_2Sal and SAM, the energy values of H_2Sal is more negative than that of SAM. So, it could be realized that H_2Sal is more stable than that of SAM which is corresponding to the higher *R*-factors of SAM as seen in Tables 1 and 5. The total optimized energy of each free molecules of H_2Sal and SAM values is only − 1.021 kcal/mol higher than cocrystal values, assuming a minimal energy for weak interaction to stabilize the cocrystal $H_2Sal{\cdot}SAM$.

The frontier molecular orbitals (FMOs) consists of the highest occupied molecular orbitals (HOMO) and the lowest unoccupied molecular orbitals (LUMO), and the (HOMO–LUMO) band-gap energy of H_2Sal, SAM and $H_2Sal{\cdot}SAM$ in atomic unit (a.u) is listed in Table 6. The molecular orbital energy may provide information on the chemical activity of the molecule, especially the ground and excited-state proton transfer processes [21]. The energy difference between the HOMO and LUMO or HOMO–LUMO gap is generally the lowest energy electronic excitation that is possible in a molecule.

Table 5 Comparision of optimization energy by B3LYP/6-311++G(d,p) method of H_2Sal, SAM and $H_2Sal{\cdot}SAM$

Compounds	Optimization energy/a.u.
H_2Sal	− 496.205829236
SAM	− 476.329560911
$H_2Sal{\cdot}SAM$	− 972.53701748
H_2Sal + SAM	− 972.535390147
ΔE{(H_2Sal + SAM)- H_2Sal –SAM}	− 0.001627333 or − 1.021 kcal mol^{-1}

Table 6 The HOMO, LUMO and HOMO–LUMO band gaps of H_2Sal, SAM and $H_2Sal{\cdot}SAM$

Compounds	HOMO/a.u.	LUMO/a.u.	Δ (HOMO)–(LUMO)/a.u./kcal mol^{-1}
H_2Sal	− 0.24577	− 0.07154	− 0.17423/− 109.33
SAM	− 0.35228	− 0.23843	− 0.11385/− 71.44
$H_2Sal{\cdot}SAM$	− 0.23701	− 0.07005	− 0.16696/− 104.7674

1 a.u. = 627.5 kcal mol^{-1}

Table 7 Electron density plot of frontier molecular orbitals of H_2Sal, SAM and $H_2Sal{\cdot}SAM$

Compound	HOMO	LUMO
H_2Sal	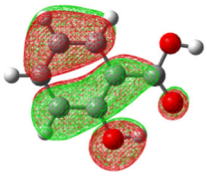 − 0.24577	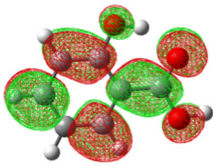 − 0.17423
SAM	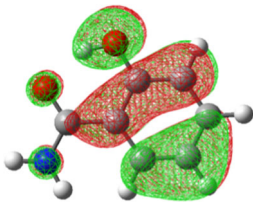 − 0.35228	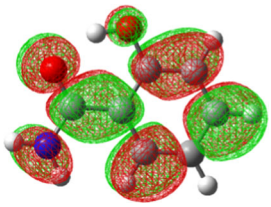 − 0.23843
$H_2Sal{\cdot}SAM$	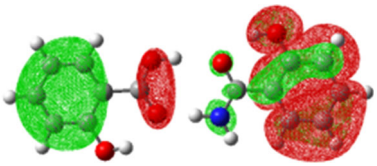 − 0.23701	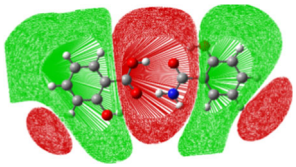 − 0.07005

Table 8 Calculated values of Mulliken atomic charges of H_2Sal, SAM and $H_2Sal{\cdot}SAM$

H_2Sal	B3LYP/6-311++G(d,p)	SAM	DFT/B3LYP/6-311++G(d,p)	H2Sal·SAM	DFT/B3LYP/6-311++G(d,p)
O11	− 0.190239	O11	− 0.394318	H2Sal O11	− 0.532523
O12	− 0.351428	O12	− 0.273489	O12	− 0.308985
O13	− 0.239083	N11	− 0.389380	N11	− 0.377387
C11	0.012887	C11	− 0.200897	C11	0.273523
C12	1.639612	C12	1.737679	C12	0.086814
C13	− 1.465100	C13	− 1.093003	C11	0.273523
C14	0.582526	C14	0.176162	C13	− 0.171249
C15	− 0.574279	C15	− 0.260867	C14	− 0.575299
C16	0.064412	C16	− 0.454859	C15	0.113373
C17	− 0.850095	C17	− 0.371454	C16	− 0.277182
H11	0.301932	H3	0.326061	C17	0.073796
H13	0.318499	H4	0.262904	H11a	0.535580
H17	0.207086	H17	0.336780	H12	0.354701
				SAM O21	− 0.251149
				O22	− 0.353894
				O23	− 0.240259
				C21	− 0.565308
				C22	1.918009
				C23	− 1.367646
				C24	0.186000
				C25	− 0.213383
				C26	− 0.213383
				C27	− 0.233971
				H21	0.440311

The atom-numbering scheme is the same as the apparent in Figs. 4–7

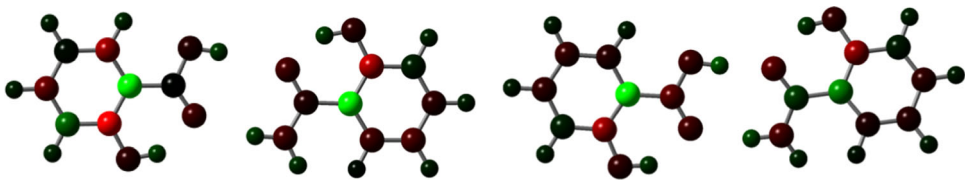

Fig. 10 Mulliken atomic charge of H_2Sal, SAM and $H_2Sal{\cdot}SAM$

The HOMO and LUMO of H_2Sal, SAM and $H_2Sal{\cdot}SAM$ are corresponding to the π orbitals whose phases are quite different which is similar to other works [21, 24]. As known, the LUMO is an electron acceptor while HOMO is electron donor [21]. In this work, the energies of the HOMO and LUMO are − 0.24577 and − 0.07154 a.u of H_2Sal, − 0.35228 and − 0.23843 a.u of SAM and − 0.23552 and − 0.07492 a.u of $H_2Sal{\cdot}SAM$. The difference between HOMO and LUMO energies are all negative values as shown in Tables 6 and 7. This is to confirm that the high stability is the large HOMO–LUMO band gap [21]. The lower value of frontier orbital energy gaps indicated intramolecular charge transfer within molecules which influence the biological activity of the molecule [21]. As seen in Table 7, the HOMO of H_2Sal, SAM and $H_2Sal{\cdot}SAM$ are the π orbitals in which electrons from the HOMO are donated [21]. The HOMO orbitals have the more electronegative atom in which the energy level is lower than others [24]. Since, the weak band of H_2Sal, SAM and $H_2Sal{\cdot}SAM$ in the observed UV spectra corresponding with $\pi \rightarrow \pi*$ are 231 nm, 235 nm and 223 nm which concerned with the transition from HOMO to LUMO are in good agreement.

DFT calculation results of Mulliken population analysis

As known, the Mulliken population charges can allow estimating the partial charges of molecules. To prove, we calculated using B3LYP level of theory with 6-311++G(d,p) basis set. Atomic charge values of optimized H_2Sal, SAM and $H_2Sal{\cdot}SAM$ molecules are listed in Table 8, and the atomic charges molecules are shown in Fig. 10.

H_2Sal molecule shows the negative charges only on O11, O12, O13, C13, C15 and C17, while the molecule of SAM shows the negative charges on O11, O12, C11, C13, C15, C16, C17 and N11. Whereas, the negative atomic charge of cocrystal $H_2Sal{\cdot}SAM$ molecules are at O21, O22, O23, C21, C23, C25, C26 and C27 for the part of H_2Sal and O11, O12, C13, C14, C16 and N11 for the part of SAM. These charges of some atoms are changing, for example, the negative charge of C11 and positive charge of C11, causing by the delocalized electrons. Undoubtedly, all the hydrogen atoms are positive electron acceptor charges. All negative charges are electron donors, corresponding with the charge transfer bonding capability [33]. The higher positive charges of H11a, H12, H13, H17 and H21 than the other hydrogen atoms plays a crucial role in the formation of the R_8^2 acid–acid dimer homosynthon, R_8^2 amide–amide dimer homosynthon, R_8^2 acid–amide dimer heterosynthon and R_{12}^4 tetramer synthon.

Conclusions

The long plate-like morphology of cocrystal of salicylic acid ($C_7H_6O_3$) and salicylamide ($C_7H_7NO_2$) or $H_2Sal{\cdot}SAM$ are obtained from the 1:2 mole ratio of salicylic acid using the solution-based method for the first time. The DSC of this cocrystal appears at the endothermic peaks corresponding to melting point at 108 °C. The molecular structures of H_2Sal, SAM are typical, whereas cocrystal $H_2Sal{\cdot}SAM$ is unique. The disordered phenolic hydroxyl (Ph-OH) of SAM in cocrystal is confirmed by single-crystal X-ray structure result, supporting an unstable, which affects the hydrogen bonds and interactions and later the complicated preparation. Moreover, these experimental structure results were calculated using DFT with 6-311++G(p,d) calculation to understand properties. The experimental and DFT calculation results are in good agreement. The stability is involved with the hydrogen synthons and weak interactions such as the R_8^2 acid–acid dimer homosynthon of H_2Sal, the R_8^2 amide–amide dimer homosynthon, the new report of R_{12}^4 amide–amide tetramer homosynthon of SAM and the R_8^2 acid–amide dimer heterosynthons of cocrystal $H_2Sal{\cdot}SAM$. The dimer phenomenon clearly confirmed the R_8^2 acid–amide dimer heterosynthons from the broad band at 2300–2800 cm^{-1} from both experimental and calculated FT-IR results and all of the positive electron acceptor charges from the Mulliken results. The experimental and DFT calculation UV results confirmed the absorbance spectra of $n \rightarrow \sigma^*$ and $\pi \rightarrow \pi*$. The calculated HOMO–LUMO energy gaps indicated the minimal energy change in cocrystal compared to an individual molecule. In addition, the lower band-gap values suggest the possible pharmaceutical activity which

is fitted well with the appearance of Flack's absolute structure parameter (0.8(18)).

Supplementary data

CCDC data 1545141-1545143 contain the supplementary crystallographic data of salicylic acid, salicylamide and cocrystal. These data can be obtained free of charge via http://www.ccdc.cam.ac.uk/conts/retrieving.html or from the Cambridge Crystallographic Data Centre, 12 Union Road, Cambridge CB2 1EZ, UK; fax: (+44) 1223-336-033; or e-mail: deposit@ccdc.cam.ac.uk.

Acknowledgements We gratefully acknowledge the Thaksin University for the research grants via the Research and Development Institute, Thaksin University (RDITSU), and the National Research Management System (NRMS); project codes: 111006 and 184788.

References

1. Brittain HG. Cocrystal systems of pharmaceutical interest: 2010. Cryst Growth Des. 2012;12:1046–54.
2. Jones W, Samuel Motherwell WD, Trask AV. Pharmaceutical cocrystals: an emerging approach to physical property enhancement. MRS Bull. 2006;31:875–9.
3. Aitipamula S, Wong ABH, Chow PS, Tan RBH. Pharmaceutical cocrystals of ethenzamide: structural, solubility and dissolution studies. Cryst Eng Commun. 2012;14:8515–24.
4. Singh M, Rai RN, Rai US. Synthesis, crystal growth and physicochemical studies on a novel organic inter-molecular compound; 3,5-dinitrobenzoic acid and salicylamide system. J Cryst Growth. 2015;419:114–22.
5. Zhou Z, Chan HK, Sung HH-Y, Tong HHY, Zheng Y. Identification of new cocrystal systems with stoichiometric diversity of salicylic acid using thermal methods. Pharm Res. 2016;33:1030–9.
6. Manin AN, Voronin AP, Drozd KV, Manin NG, Bauer-Brandl A, Perlovich GL. Cocrystal screening of hydroxybenzamides with benzoic acid derivatives: a comparative study of thermal and solution-based methods. Eur J Med Sci. 2014;65:56–64.
7. Surov AO, Manin AN, Voronin AP, Churakov AV, Perlovich GL, Vener MV. Weak interactions cause packing polymorphism in pharmaceutical two-component crystals. The case study of the salicylamide cocrystal. Cryst Growth Des. 2017;17:1425–37.
8. Évora AOL, Castro RAE, Maria TMR, Ramos Silva M, ter Horst JH, Canotilho J, Eusébio MES. A thermodynamic based approach on the investigation of a diflunisal pharmaceutical co-crystal with improved intrinsic dissolution rate. Int J Pharm. 2014;466:68–75.
9. Elbagerma MA, Edwards HGM, Munshi T, Scowen IJ. Identification of a new co-crystal of salicylic acid and benzamide of pharmaceutical relevance. Anal Bioanal Chem. 2010;397:137–46.
10. Manin AN, Voronin AP, Manin NG, Vener MV, Shishkina AV, Lermontov AS, Perlovich GL. Salicylamide cocrystals: screening, crystal structure, sublimation thermodynamics, dissolution, and solid-state DFT calculations. J Phys Chem B. 2014;118:6803–14.
11. Seato CC, Parkin A. Making benzamide cocrystals with benzoic acids: the influence of chemical structure. Cryst Growth Des. 2011;11:1502–11.
12. Nordstrom FL, Rasmuson AC. Solubility and melting properties of salicylic acid. J Chem Eng Data. 2006;51:1668–71.
13. Nordstrom FL, Rasmuson AC. Solubility and melting properties of salicylamide. J Chem Eng Data. 2006;51:1775–7.
14. Sasada Y, Takano T, Kakudo M. Crystal structure of salicylamide. Bull Chem Soc Jpn. 1964;37(7):940–6.
15. Arjunan V, Kalaivani M, Ravindran P, Mohan S. Structural, vibrational and quantum chemical investigations on 5-chloro-2-hydroxybenzamide and 5-chloro-2-hydroxybenzoic acid. Spectrochim Acta Part A. 2011;79:1886–95.
16. Bartoszek-Adamska E, Dega-Szafran Z, Krociak M, Jaskolski M, Szafran M. Hydrogen bonds in 1:1 complex of piperidine-3-carboxylic acid with salicylic acid. J Mol Struct. 2009;920:68–74.
17. Boczar M, Boda L, Wojcik MJ. Theoretical modeling of infrared spectra of hydrogen-bonded crystals of salicylic acid. Spectrochim Acta A. 2006;64:757–60.
18. Munshi P, Guru Row TN. Intra- and intermolecular interactions in small bioactive molecules: cooperative features from experimental and theoretical charge-density analysis. Acta Cryst. 2006;B62:612–26.
19. Esrafili MD. Intra- and inter-molecular interactions in salicylic acid -theoretical calculations of 17O and 1H chemical shielding tensors and QTAIM analysis. Can J Chem. 2011;89:1410–8.
20. Kwon Y. Theoretical study on salicylic acid and its analogues: intramolecular hydrogen bonding. J Mol Struct (Theochem). 2000;532:227–37.
21. Karthick T, Balachandran V, Perumal S, Nataraj A. Spectroscopic studies, HOMO–LUMO and NBO calculations on monomer and dimer conformer of 5-nitrosalicylic acid. J Mol Struct. 2011;1005:192–201.
22. Velcheva EA, Stamboliyska BA. Structural changes caused by the conversion of 2-hydroxybenzamide salicylamide into the oxyanion. J Mol Struct. 2008;875:264–71.
23. Trask AV, Jones W. Crystal engineering of organic cocrystals by the solid-state grinding approach. Top Curr Chem. 2005;254:41–70.
24. Karabacak M, Sinha L, Prasad O, Cinar Z, Cinar M. The spectroscopic (FT-Raman, FT-IR, UV and NMR), molecular electrostatic, potential, polarizability and hyperpolarizability, NBO and HOMO–LUMO analysis of monomeric and dimeric structures of 4-chloro-3,5-dinitrobenzoic acid. Spectrochim Acta Part A. 2012;93:33–46.
25. Sheldrick GM. A short history of SHELX. Acta Crystallogr Sect A. 2008;64:112.
26. Brandenburg K. Diamond. Bonn: Cryst Impact GbR; 1999.
27. Frisch J, Trucks GW, et al. Gaussian 98. Pittsburgh(PA): Gaussian Inc; 1998.
28. Rai US, Singh M, Rai RN. Some physicochemical studies on organic eutectics and intermolecular compounds. J Therm Anal Calorim. 2017;130:967–74.
29. Fernandes RP, do Nascimento ALCS, Carvalho ACS, Teixeira JA, Ionashiro M, Caires JC. Mechanochemical synthesis, characterization, and thermal behavior of meloxicam cocrystals with salicylic acid, fumaric acid, and malic acid. J Therm Anal Calorim. 2019. https://doi.org/10.1007/s10973-019-08118-7.
30. Landolt HH. Schmelzgleichgewichte, Vol. II, Part 3. 6th ed. Berlin: Springer; 1950. p. 1831–910.
31. Babhair SA, Al-Badr AA, Aboul-Enein HY. Salicylamide in analytical profiles of drug substances. In: Florey K, editor. Analytical profiles of drug substances, vol. 13. Orlando: Academic Press; 1984. p. 521–51.

32. Trivedi MK, Branton A, Trivedi D, Shettigar H, Bairwa K, Jana S. Fourier transform infrared and ultraviolet-visible spectroscopic characterization of biofield treated salicylic acid and sparfloxacin. Nat Prod Chem Res. 2015;3:1–6.
33. Amalanathan M, Rastogi VK, Hubert Joe I, Palafox MA, Tomar R. Density functional theory calculations and vibrational spectral analysis of 3,5-dinitrobenzoic acid. Spectrochim Acta Part A. 2011;78:1437–44.

Publisher's Note Springer Nature remains neutral with regard to jurisdictional claims in published maps and institutional affiliations.